

Effects of Completeness and Purity on Cluster Dark Energy Constraints

Michel Aguena^{1,*} and Marcos Lima¹

¹*Departamento de Física Matemática, Instituto de Física,
Universidade de São Paulo, CP 66318, CEP 05314-970, São Paulo, SP, Brazil*

(Dated: March 18, 2019)

The statistical properties of galaxy clusters can only be used for cosmological purposes if observational effects related to cluster detection are accurately characterized. These effects include the selection function associated with cluster finder algorithms and survey strategy. The importance of the selection becomes apparent when different cluster finders are applied to the same galaxy catalog, producing different cluster samples. We consider parametrized functional forms for the observable-mass relation, its scatter as well as the completeness and purity of cluster samples, and study how prior knowledge on these function parameters affects dark energy constraints derived from cluster statistics. Under the assumption of a **fiducial model for the selection function where completeness and purity reach 50% at masses around $10^{13.5}M_{\odot}/h$** , we find that self-calibration of selection parameters in current and upcoming cluster surveys is possible, while still allowing for competitive dark energy constraints. We consider a fiducial survey with specifications similar to those of the Dark Energy Survey (DES) with 5000 deg², maximum redshift of $z_{max} \sim 1.0$ and threshold observed mass $M_{th} \sim 10^{13.8}M_{\odot}/h$, such that completeness and purity $\sim 60\% - 80\%$ at masses around M_{th} . Perfect knowledge of all selection parameters allows for constraining a constant dark energy equation of state to $\sigma(w) = 0.033$. Employing a joint fit including self-calibration of the effective selection degrades constraints to $\sigma(w) = 0.046$. External calibrations at the level of 1% in the parameters of the observable-mass relation and completeness/purity functions are necessary to improve the joint constraints to $\sigma(w) = 0.041$. In the lack of knowledge of selection parameters, future experiments probing larger areas and greater depths suffer from stronger relative degradations on dark energy constraints compared to current surveys.

I. INTRODUCTION

The properties of dark matter halos have been characterized with increasing accuracy through dark matter N-body simulations of multiple cosmological models [1–7]. However, clusters of galaxies, observed in surveys spanning different wavelengths carry a number of observational effects [8–15]. For the cosmological use of galaxy clusters, it is necessary to understand these effects in detail (e.g. by measuring them in simulations) and use this knowledge to parametrize the effects as appropriate functions of intrinsic cluster parameters (e.g. mass and redshift). An ideal self-consistent analysis must then constrain both cosmological parameters of interest as well as *nuisance* parameters related to astrophysical and observational effects, despite intrinsic degeneracies [8–10, 16–23]. In this context, external calibrations of *nuisance* parameters may help improve constraining cosmology.

Given a set of true halos and the matter tracers associated to them (e.g. optical galaxies), the first step is to characterize the performance of algorithms for cluster identification called cluster finders. Some of these methods, such as MaxBCG[24], FoF used in [25] and RedMaPPer[26, 27], are based on the presence of red-sequence galaxies within clusters. They have the advantage of including this extra information, which is certainly valuable at low redshifts. However they may suffer

from limitations at higher redshifts. Meanwhile, there are cluster finders such as WAZP[28], VT[29] and C4[30], which rely mostly on detecting spatial overdensities. These algorithms thrive to provide better detections at higher redshifts, although they typically depend more strongly on the quality of galaxy photometric redshifts. Cluster finders may fail to identify a fraction of clusters related to dark matter halos, as well as detect false clusters with no association to halos. These two problems can be quantified by the so-called *completeness* and *purity* of the cluster sample [14, 15, 29], which typically reflect limitations of the cluster finder algorithm, such as e.g. artificial over-merging or fragmentation of clusters relative to their corresponding halos. Whereas completeness and purity may depend on various factors – such as survey specifications, the quality of photometric redshifts (photo-zs) and the observable-mass relation – they are mainly properties of the cluster finder itself. We will often refer to completeness and purity as describing the cluster selection function.

Next we must consider the *observable-mass* relation, typically characterized by a mean relation and a scatter [8, 9, 16, 17]. For optical clusters the observable is the cluster richness, representing the number of cluster member galaxies. Richness may also refer to a subsample of member galaxies whose properties more closely relate to halo mass (e.g. richness can be based on red-sequence galaxies within a cluster [26, 27], as opposed to all member galaxies). In simulations, clusters correctly matched to dark matter halos can be used to characterize the observable-mass relation [14, 31–35]. However, it is

* aguena@if.usp.br

important to point out that all of these calibrations are not enough to determine observable-mass and selection parameters at the percent level, even though they are still useful to help determine at least appropriate function forms or loose priors for parameters, which are then self-calibrated in a full cosmological analysis. Observationally, optical clusters may be matched to detections in other wavelengths (e.g. millimeter or X-ray) from which observable-observable scaling relations can be estimated [36–38], and under the assumption of hydrostatic equilibrium, observable-mass relations may be derived. Alternatively, lensing masses may be available for a fraction of the optical clusters [39–45]. In conjunction, simulations and observational cross-matches allow for independent external calibrations of the observable-mass relation.

The scatter in the observable-mass relation may also be assessed from simulations and observations, and it can be tied to different sources [13]. An intrinsic scatter exists even for a perfect cluster finder (i.e. one with unit completeness and purity) and represents instances where a cluster of given richness has a range of masses due to intrinsic variability in the physical processes that relate these quantities, turning them stochastic [31, 32]. On the other hand, imperfections in the matching of clusters may artificially change this otherwise intrinsic scatter, as well as other observational issues [13]. We will also refer to the *effective* selection function, which is characterized by a combination of the actual selection function (completeness/purity) and the observable-mass relation.

There may be an interplay between the derived observable-mass relation and the sample selection function, as the characterization of both depend on the matching process of clusters and halos (in simulations) and, clusters and clusters (in multi-wavelength observations). For instance, clusters catastrophically scattered in and out of a given richness bin may affect the sample completeness and purity, an effect which may be parametrized by altering the observable-mass distribution to include an extra Gaussian term [12]. Conversely, using only clusters and/or halos which are believed to have been correctly matched to define the observable-mass relation may produce a relation with unrealistically low scatter. Despite these issues, it is conceptually simpler to keep the definitions of completeness and purity decoupled from the observable-mass relation, and we will follow this approach in this work by parameterizing these functions independently using functional forms characterized in simulations [46].

Finally, we must characterize errors in the cluster photometric redshifts (photo-zs) [10]. We will again take the simpler approach of decoupling photo-z errors from completeness and purity issues, as photo-z errors are mainly tied to degeneracies in color-magnitude-redshift space and the efficiency of photo-z algorithms [47–49]. The selection function of cluster finders that make direct use of photo-zs [29, 43] is clearly affected by the photo-z quality, which may translate to additional sources of over-merging and fragmentation of clusters in the line-of-sight.

However, for cluster galaxies we expect the photo-z errors to be considerably smaller than for field galaxies. Therefore in this work we will neglect such effects, as our goal is to assess the direct impact of completeness and purity issues on cluster cosmology. Our analysis is conservative in this sense, since by including the extra dependencies of completeness and purity on observable-mass and photo-z parameters would effectively decrease the number of *nuisance* parameters to constrain, potentially increasing the sensitivity of cluster observables.

In this paper we study how the inclusion of the cluster sample completeness and purity impacts the cosmological constraints derived from that sample. For a given parametrization of these functions, we also explore how prior knowledge on the selection can help constrain dark energy parameters in current and upcoming galaxy surveys. We start in § II discussing the characterization of the selection function via the sample completeness and purity. In § III we discuss the formalism for predicting cluster counts and covariance, including selection effects. In § IV we detail the Fisher Matrix formalism to predict dark energy constraints and biases from cluster statistics and in § V we present the fiducial model, including selection parametrizations. In § VI we present our main results and in § VII we discuss these results and conclude.

II. COMPLETENESS AND PURITY

We define the *completeness* of a cluster catalog as the fraction of galaxy clusters *correctly* identified relative to the number of *true* dark matter halos. Likewise, the *purity* of the same catalog is defined as the fraction of galaxy clusters correctly identified relative to the *total* number of detected clusters. Clearly both concepts are important to characterize the cluster finder selection function, since nearly all algorithms lead to samples that are both incomplete and impure in certain ranges of masses and redshifts. A low completeness indicates an inefficiency of the cluster finder in detecting systems that it should have detected (or which a perfect cluster finder detects), whereas a low purity indicates a high fraction of false-positives in the sample, i.e. detections incorrectly made (and which a perfect cluster finder would not have made).

The completeness and purity of a cluster finder depend on the assumptions it makes and also on observing conditions of a specific survey. For instance, a cluster finder which uses information from the galaxy red-sequence – observed in most low-redshift clusters – has the possibility of outperforming a cluster finder that ignores this information. On the other hand, if the assumption of a red-sequence is extrapolated into a domain in which it may not apply (e.g. at higher redshifts), such cluster finder may produce samples that are either incomplete or impure. As a result, different performances may be observed when comparing different cluster finders applied to the same data set as well as the same cluster finder applied to different surveys.

From the above definitions of completeness and purity, these quantities require matching clusters to dark matter halos. Strictly speaking this can only be directly assessed in simulated catalogs, where information about the true underlying dark matter halos is fully available. However cross-checks from real observations may also provide useful hints into the selection function of a given cluster finder. Here we will assume that simulations representative of the observing conditions are available for purposes of roughly estimating the cluster finder selection function as well as the observable-mass relation. Clearly, simulations of this kind necessarily make certain assumptions that may not apply to real observed data. Nonetheless they are useful to roughly calibrate cluster finders and estimates of their selection under these assumptions. When performing a cosmological analysis on real data, one would not fully trust simulation results, but they might inspire functional forms for parameterizing the cluster selection and observable-mass relation [31, 32], whose parameter values can then be obtained from a self-consistent cosmological analysis of the cluster sample.

For pedagogical reasons, let us outline the process of using a simulated galaxy catalog and its associated dark matter halos for defining the cluster sample completeness, purity and observable-mass relation. Given the list of true dark matter halos of mass M and redshift z , and the catalog of galaxies populating these halos, one may run a cluster finder producing a list of clusters with certain observed properties (e.g. richness and photo-zs for optical clusters). Since the considerations made here apply to detections not only of optical clusters, but for multiple wavelengths, we will often refer to the *observed mass* M^{obs} instead of the direct observable \mathcal{O} . Our fiducial survey will be similar to the Dark Energy Survey (DES), so we will typically refer to the richness as the observable, derived from optical cluster finders. However, all results also apply to cluster finders defined at other wavelengths with different mass proxies. Here M^{obs} is the mass inferred from the observable, being therefore equivalent to it, but in mass units. We will formally characterize individual clusters by their values of M^{obs} and photo-z, denoted z^{phot} , and this notation applies even when we consider an specific observable such as richness. Given the number N_{h} of halos found and the number N_{c} of clusters detected, we may then consider the following steps towards characterizing the cluster finder selection function and the observable-mass distribution:

- Rank the N_{h} halos by mass M and the N_{c} clusters by richness \mathcal{O} .
- Perform a matching of halos and clusters, producing N_{mat} matches.
 - **In general the matching of halos and clusters can be done in two ways: by the fraction of coincident halo and cluster members, or by the spatial proxim-**

ity of halo and cluster centers (either 3D or angular).

- **In cases where multiple matches may potentially occur (e.g. within a cluster radius one finds more than one halo center), the most massive halo or richest cluster may be selected among the possible candidates. This assures that e.g. the most massive halo that is spatially close to the richest unmatched cluster will preferentially produce a match.**
- **A two-way matching can be applied to reassure a more stringent matching criterion. In this case the matching is made in both directions (halos are matched to clusters and vice-versa) and only pairs that coincide in both directions are kept as true matches.**

- Plot \mathcal{O} versus M for the matches to determine the observable-mass relation and its scatter. A cluster mass computed from this relation using the value of the observable \mathcal{O} represents the cluster observed mass M^{obs} .

- For each bin of halo mass M and redshift z , compute the completeness $c(M, z)$ as

$$c(M, z) = \frac{N_{\text{mat}}(M, z)}{N_{\text{h}}(M, z)}. \quad (1)$$

- For each bin of cluster observed mass M^{obs} and photo-z z^{phot} , compute the purity $p(M^{\text{obs}}, z^{\text{phot}})$ as

$$p(M^{\text{obs}}, z^{\text{phot}}) = \frac{N_{\text{mat}}(M^{\text{obs}}, z^{\text{phot}})}{N_{\text{c}}(M^{\text{obs}}, z^{\text{phot}})}. \quad (2)$$

Clearly these definitions depend on the specific matching criterion imposed in the second step above (see further discussion on a related issue in § III A). **Notice that the ranking of halos and clusters in the very first step plays only a secondary role in the matching and is in fact dispensable. It enters only as an additional criterium to resolve potential multiple matches according to physical matching criteria defined in the second step, either by membership overlap or spatial proximity.**

We may also use these matches to estimate cluster z^{phot} errors, which depend both on the quality of galaxy photo-zs and on the cluster finder performance in assigning redshifts to clusters. In this work, we will assume that the effect of photo-z errors is already encapsulated into the estimated completeness and purity and does not represent an extra source of cosmological degeneracies [10]. Obviously such assumption should be checked for each cluster finder, especially for those which heavily rely on galaxy photo-z estimates.

In observed data, the estimation of completeness and purity becomes intrinsically more complicated, as the mass of the clusters is not known and because no observed catalog can be taken as a truth table. Although the mass of the clusters can be estimated via observable-mass relations, the lack of a truth table makes the extraction of completeness and purity information from the data alone currently inviable. If reliable mock catalogs for a given survey are not available, calibration of scaling relations is possible from lensing masses measured for a fraction of the detected clusters or from matching e.g. optical clusters to detections at other wavelengths. Thus, we can obtain limited information about the observable-mass relation and its scatter. In the worst-case scenario, we could assume a generic selection function and fully self-calibrate its parameters (that is, to constrain the parameters along with the cosmology) from the observed cluster data alone. Fortunately, we expect reliable simulations, lensing masses, multiple external cross-calibrations and spectroscopic follow-ups to be available for a self-consistent cosmological analysis of most current and future cluster surveys.

III. OBSERVED CLUSTER PROPERTIES

A. Cluster Counts

We parametrize the theoretical dark matter halo mass-function as

$$\frac{d\bar{n}(z, M)}{d\ln M} = \frac{\bar{\rho}_m}{M} \frac{d\ln \sigma^{-1}}{d\ln M} f(\sigma), \quad (3)$$

where $\sigma^2(M, z)$ is the variance of the linear density field in a spherical region of radius R enclosing a mass $M = 4\pi R^3 \bar{\rho}_m / 3$ at the present background matter density $\bar{\rho}_m$. We take $f(\sigma)$ from a fit to simulations by Tinker et al [50], with parameter values appropriate for overdensity $\Delta = 200$ with respect to the background matter density. The predicted comoving number density \bar{n}_α of clusters in the observed-mass bin (indexed by α) is obtained by integrating the mass function convolved with all observational effects mentioned previously as [8–10]

$$\bar{n}_\alpha(z) = \int_{M_\alpha^{\text{obs}}}^{M_{\alpha+1}^{\text{obs}}} d\ln M^{\text{obs}} \int_0^\infty d\ln M \frac{d\bar{n}_{\text{obs}}}{d\ln M}, \quad (4)$$

where the *observed* mass-function

$$\frac{d\bar{n}_{\text{obs}}}{d\ln M} = \frac{d\bar{n}(z, M)}{d\ln M} P(M^{\text{obs}}|M) \frac{c(M, z)}{p(M^{\text{obs}}, z^{\text{phot}})} \quad (5)$$

carries the effects of completeness, purity and observable-mass distribution $P(M^{\text{obs}}|M)$, assumed to be Gaussian in $\ln M$. The number counts in the i^{th} photo- z bin are then obtained by integrating the comoving number density in comoving volume or redshift, including the photo- z error distribution as [10]

$$\bar{m}_{\alpha, i} = \int_{z_i^{\text{phot}}}^{z_{i+1}^{\text{phot}}} dz^{\text{phot}} \int_0^\infty dz P(z^{\text{phot}}|z) \frac{r^2(z)}{H^2(z)} \bar{n}_\alpha(z) \quad (6)$$

where $H(z)$ is the Hubble parameter at redshift z and $r(z)$ is the comoving angular diameter distance, identified here with the comoving radial distance since we only consider flat cosmologies. As mentioned previously, we will not consider the effect of photo- z errors explicitly here. In the above description, this implies taking $P(z^{\text{phot}}|z)$ to be a Dirac delta function, which then allows us to perform one of the redshift integrals trivially. In this case, we denote the *effective* cluster selection $f(M^{\text{obs}}|M)$ as the combination

$$f(M^{\text{obs}}, z|M) = P(M^{\text{obs}}|M) \frac{c(M, z)}{p(M^{\text{obs}}, z)}. \quad (7)$$

The separation of f into these three components is mostly pedagogical, as the effective selection itself can be measured directly from simulations (with no reference to separate components). In fact, it is possible to consider completeness and purity effects (partially) as a propagation of projection effects into the otherwise intrinsic observable-mass relation $P(M^{\text{obs}}|M)$, turning it into $f(M^{\text{obs}}|M)$ [12]. Whereas simulations indicate that $P(M^{\text{obs}}|M)$ can be parametrized as a log-gaussian distribution [31–33, 38, 45, 51] with observable-mass relations displaying low scatter [32], $f(M^{\text{obs}}|M)$ would then have an extra log-gaussian component, turning the final distribution to be non-log-gaussian [12].

Projection effects occur mainly as a result of photometric redshift errors, which cause cluster finders to fail in multiple ways. The simplest failure mode is when the cluster finder still detects individual clusters appropriately, but either includes field galaxies as cluster members or excludes true cluster members. In this case, projection effects conserve the total number of clusters and act merely as an extra source of scatter for richness estimates and could indeed be modeled as an extra log-gaussian component for the observable-mass distribution. However, in more extreme cases of failure, the cluster finder may inappropriately fragment one cluster into two, merge two separate clusters along the line of sight into a single cluster, or simply fail to find a cluster due to poor signal-to-noise. These failure modes do not conserve the number of clusters and more strongly affect the measured cluster counts and variance. Our parametrization of selection in terms of completeness and purity attempts to capture all these possible cluster-finder failure modes.

As mentioned before, the observable-mass relation $P(M^{\text{obs}}|M)$ has an intrinsic scatter due the physical processes that correlate these quantities. This scatter can be studied and quantified in simulations, being well understood. However, there is an additional source of scatter related to the use of observed mass and richness on $P(M^{\text{obs}}|M)$. When calibrating $P(M^{\text{obs}}|M)$, the uncertainties on the measurement of both the richness and the mass also have to be included [38]. For simplicity, we will not consider this extra observational effect.

However, contamination by projection effects is not the only issue that may affect the total selection. One simple effect, which however is likely always present, is a

mismatch between the effective overdensity Δ_c used to define observed clusters and the overdensity Δ_h of the dark matter halos associated to them (either halos directly matched to clusters in simulations or halos whose mass-function is used to predict the cluster abundance). For instance, if we use a halo mass-function appropriate for Δ_h to predict the *cluster* abundance as described above, but our cluster finder detects clusters at an effective overdensity $\Delta_c \neq \Delta_h$, a mismatch of halo and cluster properties will follow if not accounted for explicitly. Notice that these effects may happen even for a perfect cluster finder, and because they are associated to the cluster detection itself, they cannot be corrected after detection by simply redefining cluster masses with a more appropriate overdensity or even a new observable. For clusters detected using signal-to-noise ratios or fixed apertures, which do not correspond to a fixed halo overdensity, it may be even trickier to interpret comparisons of cluster and halo properties.

From the considerations above, it is clear that completeness and purity depend on specific assumptions underlying cluster finder algorithms. In this work we will parametrize the selection via separate functions for the sample completeness and purity as described in § V.

B. Cluster Covariance

The local number counts $m_{\alpha,i}(\mathbf{x})$ of clusters at position \mathbf{x} fluctuate spatially around the mean predicted values $\bar{m}_{\alpha,i}$, following the matter density contrast $\delta(\mathbf{x})$ as

$$m_{\alpha,i}(\mathbf{x}) = \bar{m}_{\alpha,i}[1 + b_{\alpha}(z)\delta(\mathbf{x})], \quad (8)$$

where $b_{\alpha}(z)$ is the average cluster bias defined as

$$b_{\alpha}(z) = \frac{1}{\bar{n}_{\alpha}(z)} \int_0^{\infty} d \ln M \frac{d\bar{n}_{\alpha}}{d \ln M} b(M, z). \quad (9)$$

Notice that $b_{\alpha}(z)$ is consistently predicted from the number density in Eq. 4, and therefore carries the observable-mass and selection effects. Here $b(M, z)$ is the halo bias for which we will take a fit to simulations by Tinker et al. 2010 [52] as

$$b(M, z) = 1 - A \frac{\nu^a}{\nu^a + \delta_c^a} + B\nu^b + C\nu^c, \quad (10)$$

where $\nu(M, z) = \delta_c/\sigma(M, z)$, $\delta_c = 1.686$ and we fix values for the parameters A, B, C, a, b, c appropriate for the same overdensity $\Delta = 200$ used in the abundance predictions.

The cluster counts have a sample covariance $S_{ij}^{\alpha\beta}$ due to the large scale structure of the Universe given by [9, 53]

$$\begin{aligned} S_{ij}^{\alpha\beta} &= \langle (m_{\alpha,i} - \bar{m}_{\alpha,i})(m_{\beta,j} - \bar{m}_{\beta,j}) \rangle \\ &= \bar{m}_{\alpha,i} b_{\alpha,i} \bar{m}_{\beta,j} b_{\beta,j} \int \frac{d^3k}{(2\pi)^3} P(k) W_i^*(\mathbf{k}) W_j(\mathbf{k}), \end{aligned} \quad (11)$$

where $W_i(\mathbf{k})$ is the Fourier transform of the volume window function in bin i and we set $b_{\alpha,i} \approx b_{\alpha}(z_i)$ at the bin centroid z_i , which is valid for sufficiently small redshift bins.

Here we will take a window to be a cylinder with a small angular radius ($\theta_s \lesssim 10$ deg) and height δr_i , in which case $W_i(\mathbf{k})$ is given by [10, 54]

$$W_i(\mathbf{k}) = 2 \exp(ik_{\parallel} r_i) j_0 \left(\frac{k_{\parallel} \delta r_i}{2} \right) \frac{J_1(k_{\perp} \theta_s r_i)}{k_{\perp} \theta_s r_i}, \quad (12)$$

where $\mathbf{k} = (k_{\parallel}, \mathbf{k}_{\perp})$. The counts are also subject to Poisson variance or shot noise given by

$$M_{ij}^{\alpha\beta} = \delta_{\alpha\beta} \delta_{ij} \bar{m}_{\alpha,i}, \quad (13)$$

such that the total covariance $C_{ij}^{\alpha\beta}$ is the sum of sample covariance and Poisson variance

$$C_{ij}^{\alpha\beta} = S_{ij}^{\alpha\beta} + M_{ij}^{\alpha\beta}. \quad (14)$$

IV. FISHER MATRIX

We use the Fisher matrix formalism to study the effects of parametrizing the cluster selection function, given the predictions of cluster counts and covariance described in the previous section. We split the counts in redshift, mass and angular cells. For convenience of notation, we let the index i denote binning in photo- z , observed mass and angular pixel, and arrange the counts into a single vector $\bar{\mathbf{m}}$. Similarly we arrange the sample covariance, Poisson variance and total covariance of $\bar{\mathbf{m}}$ into matrices \mathbf{S} , \mathbf{M} and $\mathbf{C} = \mathbf{S} + \mathbf{M}$.

Given a set of parameters θ_{α} , the Fisher matrix quantifies the information in both the cluster counts and cluster covariance as [9, 10]

$$F_{\alpha\beta} = \bar{\mathbf{m}}_{,\alpha} \mathbf{C}^{-1} \bar{\mathbf{m}}_{,\beta}^T + \frac{1}{2} \text{Tr} [\mathbf{C}^{-1} \mathbf{S}_{,\alpha} \mathbf{C}^{-1} \mathbf{S}_{,\beta}], \quad (15)$$

where the first term contains information on the counts and the second term the information on the covariance of these counts. The clustering properties of galaxy clusters - encoded in their covariance - bring extra information to the cluster counts, which helps on self-calibration (constraining *nuisance* parameters along with the cosmology) of observable-mass distribution [9, 10, 17, 18, 51] and, as we shall see, of the cluster selection function. The inverse Fisher matrix approximates the covariance matrix of the parameters $C_{\alpha\beta} \approx [F^{-1}]_{\alpha\beta}$. The marginalized error on a single parameter θ_{α} is $\sigma(\theta_{\alpha}) = [F^{-1}]_{\alpha\alpha}^{1/2}$. In case we have *prior* information on parameter θ_{α} at the level of $\sigma_p(\theta_{\alpha})$, we add to the Fisher matrix a diagonal contribution of $\sigma_p^{-2}(\theta_{\alpha})\delta_{\alpha\beta}$ before inversion.

Finally, variations on the number counts of $\Delta\bar{\mathbf{m}}$ and on the sample covariance of $\Delta\mathbf{S}$, relative to their values in the fiducial model, induce a systematic error or bias

$b(\theta_\alpha) = \delta\theta_\alpha$ on a derived parameter θ_α , given by [12, 55]

$$b(\theta_\alpha) = F_{\alpha\beta}^{-1} \left\{ \bar{\mathbf{m}}_{,\beta} \mathbf{C}^{-1} \Delta \bar{\mathbf{m}} + \frac{1}{2} \text{Tr} [\mathbf{C}^{-1} \mathbf{S}_{,\beta} \mathbf{C}^{-1} \Delta \mathbf{S}] \right\}. \quad (16)$$

This equation can be used for assessing the bias on inferred cosmological parameters when neglecting the inclusion of selection function parameters, given that the true counts in the fiducial model require these additional parameters.

V. FIDUCIAL MODEL

We choose a fiducial cosmology from a flat w CDM model with best-fit parameters consistent with the results from Planck [56], as $h^2\Omega_m = 0.14$, $h^2\Omega_b = 0.022$, $w = -1$, $A_s = 2.13 \times 10^{-9}$ (corresponding to $\sigma_8 = 0.83$), $n_s = 0.96$, $\tau = 0.089$. We also set priors of 1% on all parameters, except for the $h^2\Omega_m$ and w , which will vary freely as we wish to study the potential for galaxy clusters to constrain dark energy in the presence of cluster selection parameters.

We assume a survey area of 5000 deg², similar to that planned for the final observations of the Dark Energy Survey (DES) [57]. We consider the counts and covariance within 500 cells of 10 deg² each. To reflect expectations and limitations of cluster finders in current optical surveys, we restrict the analysis to 9 redshift bins of $\Delta z = 0.1$ from $z = 0.1$ to $z_{max} = 1.0$. We also include seven bins of observed mass of $\Delta \log[M^{\text{obs}}/(M_\odot h^{-1})] = 0.2$ from a threshold mass of $M_{th}^{\text{obs}} = 10^{13.8} M_\odot/h$, where the last bin was reshaped to $\log[M^{\text{obs}}/(M_\odot h^{-1})] = [15.0 : 17.0]$ to include all high-mass clusters. This binning choice leaves us with 63 bins of count measurements, which we expect to be sufficient for providing information on the observed mass and redshift evolution of the selection function and the observable-mass relation. The completeness and purity mostly shift each bin individually (although to consider the full effect of completeness within an observed mass bin it is necessary to integrate over all masses, see Fig. 1). The scatter on the observable-mass relation spreads a portion of the clusters across different mass bins, and the mass bias systematically shifts clusters to higher (or lower) observed mass bins. This approach also allows us to test the cluster constraining power when considering different minimum masses, by simply adding (or removing) mass bins.

The observable-mass $P(M^{\text{obs}}|M)$ distribution will be assumed to be Gaussian in $\ln M$ with a scatter $\sigma_{\ln M}$ and bias $\ln M_{bias}$

$$P(M^{\text{obs}}|M) = \frac{1}{\sqrt{2\pi\sigma_{\ln M}^2}} \exp \left[-\frac{\chi^2(M^{\text{obs}})}{2} \right] \quad (17)$$

where

$$\chi(M^{\text{obs}}) = \frac{\ln M^{\text{obs}} - \ln M - \ln M_{bias}}{\sigma_{\ln M}}. \quad (18)$$

We parametrize the evolution of the mass bias with redshift as [9],

$$\ln M_{bias}(z) = A_b + n_b \ln(1+z), \quad (19)$$

where the fiducial values are $A_b = n_b = 0$. Since we expect the mass scatter in the relation to increase for high redshifts and low masses, we take

$$\frac{\sigma_{\ln M}^2(z, M)}{0.2^2} = 1 + B_0 + B_z(1+z) + B_M \left(\frac{\ln M_s}{\ln M} \right), \quad (20)$$

with the fiducial values of $B_0 = B_z = B_M = 0$ and we fix the pivot mass $M_s = 10^{14.2} M_\odot/h$.

As clusters of high mass stand out in observations, we expect less ambiguity in detecting them. Therefore the completeness and purity should approach unity at high enough values of M and M^{obs} . Similarly, for low masses, the number of clusters increase and we expect the confusion to be larger, so the completeness and purity decrease. We set a functional form for both completeness and purity that interpolates between these two limits of high and low masses as

$$c(M, z) = \frac{[M/M_c(z)]^{n_c}}{[M/M_c(z)]^{n_c} + 1}, \quad (21)$$

$$p(M^{\text{obs}}, z^{\text{phot}}) = \frac{[M^{\text{obs}}/M_p^{\text{obs}}(z)]^{n_p}}{[M^{\text{obs}}/M_p^{\text{obs}}(z)]^{n_p} + 1}, \quad (22)$$

where $M_c(z)$ and $M_p(z)$ are parametrized functions and we take the exponents n_c and n_p to be constants. This functional form was characterized and shown to describe well completeness and purity in simulations [46]. We consider 2 different cases, as shown in Table I: case (1) sets values $n_c = 3$ and $n_p = 1$, therefore the ratio c/p goes to zero in the limit of low M and M^{obs} ; case (2) sets values $n_c = 1$ and $n_p = 3$, therefore the ratio c/p goes to infinity in the limit of low M and M^{obs} . These two cases should bracket a reasonable range of possible parametrizations for the selection and their dependence on mass and redshift. For the mass scales M_c and M_p^{obs} , which control the transition in completeness and purity function, we take linear relations:

$$\log M_c(z) = \log \tilde{M}_c + c_0 + c_1(1+z) \quad (23)$$

$$\log M_p^{\text{obs}}(z) = \log \tilde{M}_p^{\text{obs}} + p_0 + p_1(1+z) \quad (24)$$

with fiducial values of $c_0 = p_0 = c_1 = p_1 = 0$. Here \tilde{M}_c and \tilde{M}_p^{obs} are arbitrary pivot masses where completeness and purity decrease to 50% in the fiducial model. For illustrative purposes we fix them to $\tilde{M}_c = 10^{13.6} M_\odot/h$ and $\tilde{M}_p^{\text{obs}} = 10^{13.5} M_\odot/h$, which results in completeness \approx (80%, 61%) and purity \approx (67%, 89%) around the threshold mass for cases (1,2).

For reference, we consider an additional case of perfect cluster detection, i.e. completeness and purity equal to

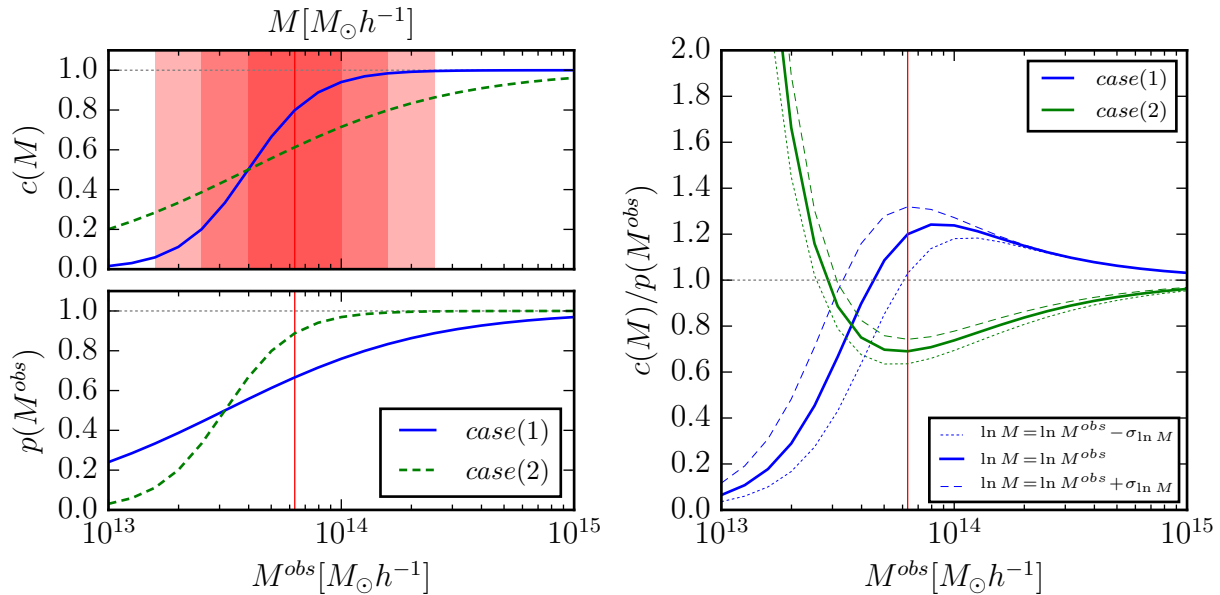


FIG. 1. Completeness and purity as a function of mass for cases (1) and (2) at $z = 0$. The red vertical line denotes the threshold mass $M_{th}^{obs} = 10^{13.8} M_{\odot}/h$ assumed in the fiducial model. (Left): both functions are shown separately and the red shaded regions display the mass spread around this threshold at 1, 2 and $3\sigma_{\ln M}$. (Right): Ratio of completeness and purity (see Eq. 7) as a function of mass. As a result, case (1) produces an increase on cluster counts for higher masses and a decrease at lower masses, while case (2) induces the opposite behavior.

unit for all masses and redshifts. We will denote this as case (0) and will consider the bias induced on dark energy parameters when case (0) is assumed whereas the true model is either case (1) or (2). We will also consider the dark energy constraints derived within cases (1) and (2) and the impact of prior knowledge on *nuisance* parameters describing the observable-mass relation and cluster selection.

The functional forms proposed for completeness and purity are shown on the left panel of Fig. 1. While purity is a function of the observed mass of clusters, completeness depends on true mass of the dark matter halos. Therefore for a given value of observed mass, the effective completeness results from the contribution of a range of true masses determined by the scatter in the observable-mass relation. This feature is illustrated on the left panel of Fig. 1, where the vertical red line indicates the fiducial observed mass threshold $M_{th}^{obs} = 10^{13.8} M_{\odot} h^{-1}$, and the red shaded regions delineate the scatter at 1, 2 and $3\sigma_{\ln M}$ levels for the effective selection.

The right panel of Fig. 1 shows the ratio of completeness and purity (c/p), which affects the effective cluster selection in Eq. 7. For each of the cases (1) and (2), the ratio c/p has limits indicated in Table I. In both cases, the ratio $c/p \rightarrow 1$ in the limit of high masses, since both c and p approach unit in this limit. For case (1) the ratio $c/p \rightarrow 0$ at lower masses; however, in the mass range investigated ($\geq 10^{13.8} M_{\odot} h^{-1}$), the ratio $c/p > 1$, resulting in more detected clusters than case (0). An opposite effect occurs for case (2), resulting in fewer cluster detections. Although the region of very low masses

Case	completeness	purity	c/p (as $M \rightarrow 0$)
0	$c = 1$	$p = 1$	1
1	$n_c=3$	$n_p=1$	0
2	$n_c=1$	$n_p=3$	∞

TABLE I. Cases considered for completeness and purity parameter values.

($M^{obs} \sim 10^{13} M_{\odot} h^{-1}$) is not the focus of this work, it is interesting to analyze what happens to the ration c/p in this limit. For case (1), the completeness decreases faster than the purity, meaning that the capability of the cluster finder detect objects goes to zero. The other case, where c/p becomes large at low masses, happens when purity decreases faster than completeness. This may happen for instance as the cluster finder attempts to detect clusters whose BCG has magnitude close to the survey limiting magnitude, particularly at low masses and high redshifts. As the cluster finder struggles with the detection, the number of false positives may become larger than the number of missed clusters.

Notice that by using multiple observables, we attempt to self-calibrate various nuisance parameters describing the observable-mass relation and the selection effects. In reality, this will only be effective if the parametrizations used are indeed correct.

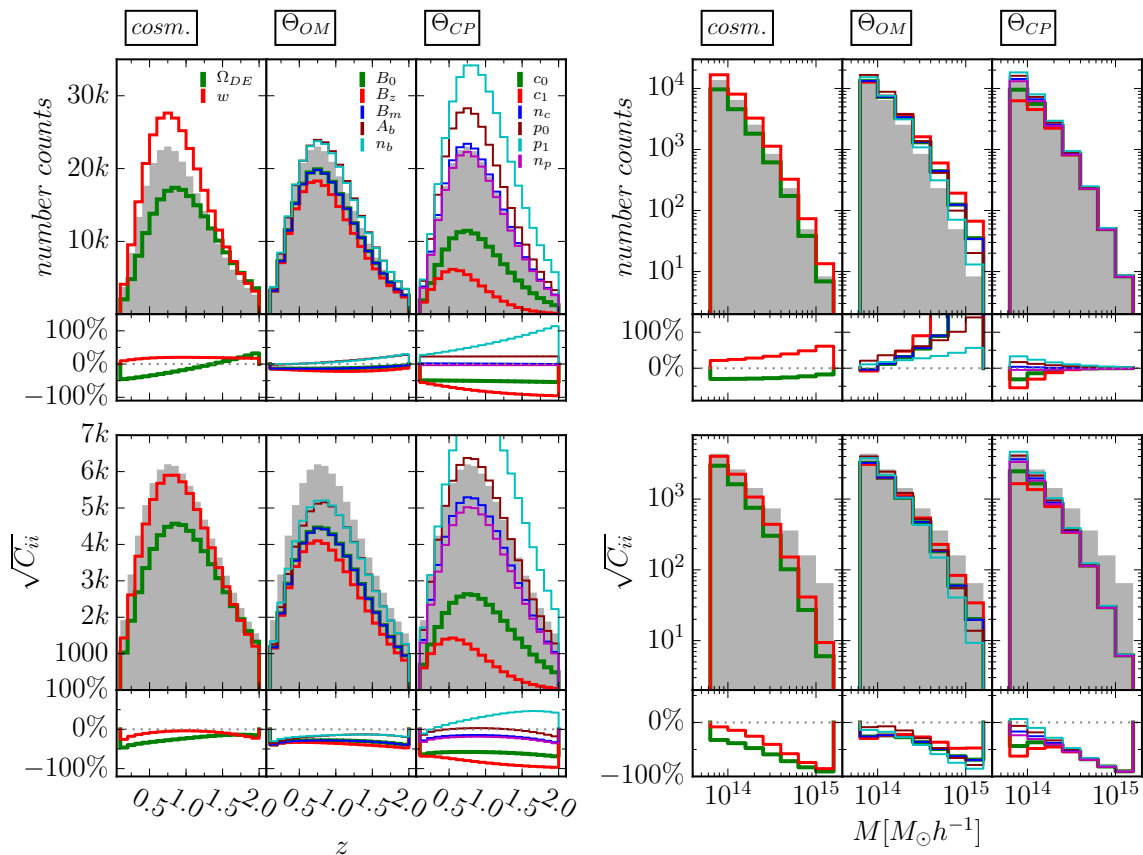


FIG. 2. Variation of the cluster number counts (*top*) and sample variance (*bottom*) as a function of redshift (*left*) and mass (*right*) for changes in parameters of dark energy, observable-mass relation and completeness and purity, considering case (1). The left panels were computed for the mass bin $M_{th}^{obs} = [13.8 : 14.0]$ and the right panels for the redshift bin $z = [0.6, 0.7]$. The gray shaded region is the fiducial case, and the colored lines indicate a variation of +0.2 in each parameter.

VI. RESULTS

Before studying the impact of selection parameters on dark energy constraints, for illustrative purposes we first look at the effect on cluster abundance and clustering from each cosmological and *nuisance* parameter. Fig. 2 shows the effects of cosmology and selection on the number counts (top) and the diagonal of sample covariance (bottom) as a function of redshift (left) and mass (right), with selection parameters from case (1). The left panels, where different redshift bins are displayed, were computed in the mass bin $M_{th}^{obs} = [13.8 : 14.0]$, and the right panels in the redshift bin $z = [0.6, 0.7]$, as those are the bins with the largest number of objects, having a more significant contribution on the constraints. We note that the actual constraining results make use of all mass and redshift bins and the non-diagonal terms of the sample covariance. We compute counts for the fiducial model (gray shaded region) and for positive variations of 0.2 in each parameter considered.

To evaluate some of the effects the parameters considered have on the constraints, let us explore the changes on the number counts as a function of redshift (top left

panel of Fig. 2). We assume a flat universe, so an increase in Ω_{DE} results in a reduction for Ω_m and the overall abundance of clusters is reduced. Increasing w causes the dark energy behavior to be closer to that of non-relativistic matter, also resulting in an increase on cluster counts.

From the definition of mass bias M_{bias} in Eq. 18, increasing its value results in a lower effective mass threshold, therefore increasing the counts of clusters. The same is true for the mass scatter [9], though with a lower sensitivity compared to the mass bias.

Increasing the completeness parameters c_0 and c_1 increases the mass scale M_c in which completeness becomes 50%, lowering the values of completeness across all masses and reducing the counts of detected clusters. An increase on n_c makes the drop in completeness at $M < M_c$ sharper, resulting in a slight increase of completeness for $M > M_c$ and a decrease for $M < M_c$. Since the mass threshold adopted ($M_{th}^{obs} = 10^{13.8} M_{\odot} h^{-1}$) is higher than the fiducial value of M_c ($10^{13.5} M_{\odot} h^{-1}$), increasing n_c produces a slight increase in the counts.

Finally, given our effective cluster selection from Eq. 7, purity has an inverse effect compared to the the com-

pleteness for the counts. In fact, since completeness and purity have the same functional form, changes in each purity parameter causes opposite effects on counts compared to changes in the corresponding completeness parameter.

These results indicate how parameters are (anti) correlated, i.e. how changes in one parameter can compensate for changes in other parameters. These effects, however, reflect the dependency around the fiducial model when fixing all other parameters at their fiducial value. When marginalizing over parameters, the resulting correlations may change.

A. Selecting Cases

The first issue we consider is whether it is worth including completeness and purity parameters in the cluster analysis for purposes of constraining dark energy. Including extra *nuisance* parameters (related to the observational effects) increases the accuracy, but decreases the precision of cosmological constraints. When completeness and purity effects are ignored, i.e. when case (0) is assumed despite imperfect selection, the resulting cosmological parameters θ_α constrained have a bias $b(\theta_\alpha)$ (Eq. 16). The assumption of perfect detection can still provide reliable cosmological parameter constraints as long as the bias is smaller than the parameter constraints

$$b(\theta_\alpha) \lesssim \gamma\sigma(\theta_\alpha) = \gamma (F^{-1})_{\alpha\alpha}^{1/2}, \quad (25)$$

where $\gamma = 1, 2, 3$ indicate biased predictions inside the 68, 95, 99% confidence levels. Here $\Delta\bar{\mathbf{m}}$ and $\Delta\mathbf{S}$ in Eq. 16 are the differences in counts and sample covariance between predictions in case (0) and cases (1,2).

Fig. 3 shows the bias induced on dark energy parameters (Ω_{DE}, w) as a function of the observed mass threshold used M_{th}^{obs} , if we assume case (0) when in reality counts are described by case (1) (solid line) and (2) (dashed line). Also shown are the 1,2 and 3 σ confidence levels on (Ω_{DE}, w) in case (0) (blue shaded regions). This observed mass threshold we consider does not imply that only a single bin of mass is being used, but that mass bins of $\Delta \log[M^{obs}/(M_\odot h^{-1})] = 0.2$ down to this threshold are being used. Therefore, $\log[M_{th}^{obs}/(M_\odot h^{-1})] = 13.8$ results in 7 observable mass bins, while $\log[M_{th}^{obs}/(M_\odot h^{-1})] = 14.2$ considers only 5 observable mass bins. The bias on Ω_{DE} has surpassed the 1 σ constraints for thresholds $\log[M_{th}^{obs}/(M_\odot h^{-1})] \leq 14.2$ in both cases (1) and (2). In fact, the bias is larger than 2 σ for case (1) and 3 σ for case (2) around the fiducial threshold mass $\log[M_{th}^{obs}/(M_\odot h^{-1})] = 13.8$. The bias on w is around 1 σ at $\log[M_{th}^{obs}/(M_\odot h^{-1})] = 13.8$, indicating that this parameter is less sensitive to the selection effects. However w is less well constrained than Ω_{DE} so a bias comparable to 1 σ constraints may be even more significant when constraining models of dark energy.

Notice that the bias behavior as a function of M_{th}^{obs} is not monotonic. This occurs mainly due to the fact that

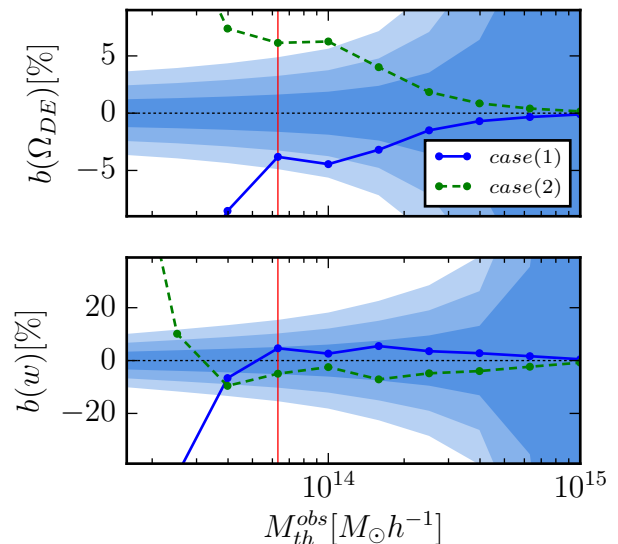


FIG. 3. Comparison between i) the 1, 2, 3 σ constraints (blue shaded regions) on dark energy parameters $\theta_{DE} = (\Omega_{DE}, w)$ for case (0) of perfect cluster selection and the ii) percent bias $b(\theta_{DE})$ (lines) on dark energy caused by ignoring completeness and purity effects as given by cases (1,2) (solid, dashed). As the bias becomes comparable to 1 σ constraints $b(\theta_\alpha) \approx \sqrt{F_{\alpha\alpha}^{-1}}$, the assumption of perfect detection results in significantly incorrect best-fit predictions. For the threshold mass considered of $\log[M_{th}^{obs}/(M_\odot h^{-1})] = 13.8$ (vertical red line), the bias $b(\Omega_{DE})$ is larger than the corresponding 2 σ constraint for both cases (1,2), whereas $b(w)$ is comparable to the 1 σ constraint.

the ratio c/p of completeness and purity is also not monotonic, as seen on the right panel of Fig. 1. For very large thresholds c/p indeed approaches unit, as in case (0) and the bias is small. For masses around the fiducial threshold, the bias is caused mainly by the upper/lower bump in c/p for case (1)/(2). For lower masses, the bias becomes much larger and is dominated by the rapid change in c/p for both cases (1) and (2).

Given that the minimum mass threshold that still allows for somewhat reliable dark energy constraints under case (0) is located at $14.2 < \log[M_{th}^{obs}/(M_\odot h^{-1})] < 14.4$, we now investigate for what mass thresholds the constraints under cases (1) and (2) become better than those from case (0) under $\log[M_{th}^{obs}/(M_\odot h^{-1})] = 14.2$ as a conservative comparison. As we go to lower threshold masses and need to fully model the selection with a larger number of *nuisance* parameters (describing completeness and purity), we also increase considerably the number of clusters probed, which brings more cosmological information.

The left panel of Fig. 4 shows 1 σ constraints for cases (0), (1) and (2) as a function of the observed mass threshold M_{th}^{obs} . The dotted lines mark the mass threshold $\log[M_{th}^{obs}/(M_\odot h^{-1})] = 14.2$ and the corresponding con-

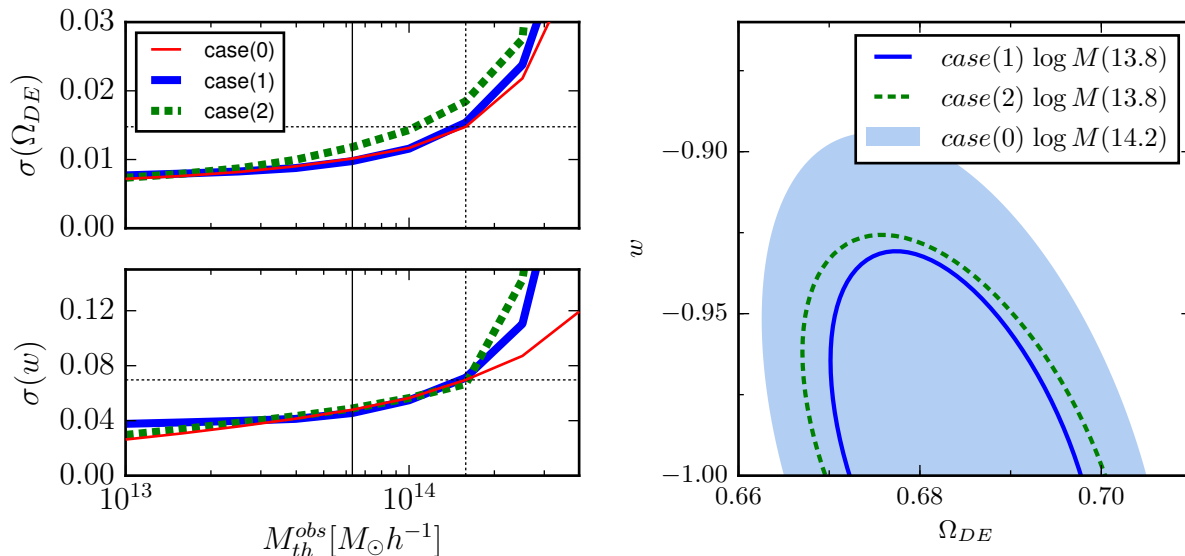


FIG. 4. (Left): Constraints on dark energy parameters (Ω_{DE}, w) as a function of threshold mass for different cases (0), (1) and (2). Even though the constraints are somewhat similar, for case (0) they are only reliable down to $\log[M_{th}^{obs}/(M_{\odot}h^{-1})] = 14.2$ (dotted vertical line). (Right): Constraints for cases (0),(1) and (2) at different threshold masses. The blue shaded region shows constraints for case (0) under its minimum threshold $\log[M_{th}^{obs}/(M_{\odot}h^{-1})] = 14.2$. Both cases (1) and (2), which include completeness and purity and go to a lower threshold $\log[M_{th}^{obs}/(M_{\odot}h^{-1})] = 13.8$, produce better constraints than case (0).

straints for case (0). As we decrease the threshold mass, the constraints for cases (1,2) improve. At the fiducial threshold $\log[M_{th}^{obs}/(M_{\odot}h^{-1})] = 13.8$, the marginalized constraints of Ω_{DE} and w for both cases (1) and (2) are lower than those from case (0) with threshold $\log[M_{th}^{obs}/(M_{\odot}h^{-1})] = 14.2$.

The right panel of Fig. 4 shows the joint dark energy constraints for multiple cases at different thresholds. The solid and dashed lines correspond to cases (1) and (2) respectively with the fiducial threshold, whereas the blue shaded region corresponds to case (0) and the higher threshold in which this case is marginally reliable. We see that a fiducial threshold $\log[M_{th}^{obs}/(M_{\odot}h^{-1})] = 13.8$ is enough to significantly improve dark energy constraints relative to case (0), despite the increase in the number of *nuisance* parameters from the selection function.

It is interesting to notice that, as we consider even lower threshold masses than the fiducial one assumed here, we continue to improve dark energy constraints. However that requires us to trust that the selection can still be well described by the parametrized functional forms assumed here down to those lower masses. That assumption has to be backed up by multiple methods, including trustworthy simulations and comparisons to other cluster detections at multiple wavelengths. Using a slightly incorrect selection at low masses could highly bias the derived constraints. More conservatively, in going to lower masses, one needs to consider more general forms for the selection with increasing number of *nuisance* parameters (modeling the selection function and mass-richness relation), which would likely degrade cos-

θ_{OM}	θ_{CP}	Case (1)		Case (2)	
		$\sigma(\Omega_{DE})$	$\sigma(w)$	$\sigma(\Omega_{DE})$	$\sigma(w)$
fix	fix	0.006	0.033	0.006	0.036
free	fix	0.009	0.044	0.010	0.047
fix	free	0.009	0.042	0.010	0.045
free	free	0.010	0.046	0.012	0.049
1%	free	0.009	0.042	0.010	0.045
free	1%	0.009	0.044	0.010	0.048
1%	1%	0.006	0.041	0.007	0.042

TABLE II. Constraints on dark energy parameters (Ω_{DE}, w) for different prior on observable-mass parameters θ_{OM} and completeness/purity parameters θ_{CP} .

mological constraints.

It becomes clear nonetheless that if one can properly model the survey completeness and purity down to levels of around $\sim 60\%$ – for which the assumption of perfect selection can no longer be made – the information in cluster counts and clustering is enough to self-calibrate observable-mass and selection parameters (constrain the parameters along the cosmology), providing better dark energy constraints than fixing conservatively higher thresholds in order to ignore selection effects.

B. Completeness and Purity Effects

In this section, for illustrative purposes we focus our discussion on the constraints from case (1), but the results and conclusions for case (2) are similar (see e.g. Table II). We start considering baseline constraints for the fiducial model described in § V, assuming perfect knowledge of the observable-mass relation as well as the completeness and purity. In this case the dark energy constraints are $\sigma(\Omega_{\text{DE}}, w) = (0.006, 0.033)$. If we let the observable-mass parameters vary freely, but keep the completeness/purity parameters fixed, these constraints degrade to $(0.009, 0.044)$.

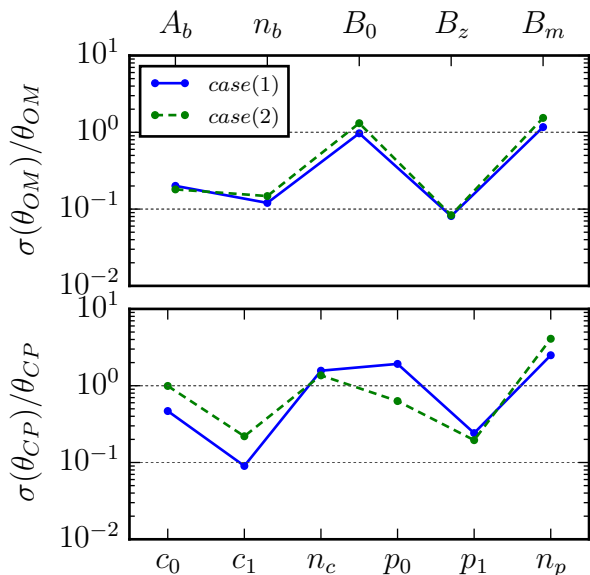


FIG. 5. Fisher constraints derived for *nuisance* parameters in case (1) (blue solid line) and case (2) (green dashed line). The parameters are related to the observable-mass relation (*top panel*) and completeness/purity (*bottom panel*). No priors were assumed for these *nuisance* parameters.

Next, we consider the effect of varying the parameters of completeness and purity. First we fix the observable-mass parameters and let completeness/purity parameters vary freely. In this case the dark energy constraints become $(0.009, 0.042)$. If we now let both the observable-mass and completeness/purity parameters vary freely, the constraints become $(0.010, 0.046)$. This corresponds to a degradation of (70%, 36%) relative to the case where these functions are perfectly known, but of only (4%, 2%) relative to the case where only the selection is fixed. Therefore, including completeness and purity effects on top of observable-mass parameters avoids biased parameters without degrading the constraints significantly.

Finally, in order to quantify the effects of priors $\sigma_p(\theta_n)$ assumed on *nuisance* parameters $\theta_n = (\theta_{\text{OM}}, \theta_{\text{CP}})$, namely observable-mass parameters θ_{OM} and/or completeness/purity parameters θ_{CP} , we define the degradation factor $\mathcal{D}_{\theta_{\text{DE}}}$ on the constraints of dark energy pa-

rameters $\theta_{\text{DE}} = (\Omega_{\text{DE}}, w)$ as

$$\mathcal{D}_{\theta_{\text{DE}}}[\sigma_p(\theta_n)] = \frac{\sigma[\theta_{\text{DE}}|\sigma_p(\theta_{\text{OM}}), \sigma_p(\theta_{\text{CP}})]}{\sigma(\theta_{\text{DE}})|_{\text{ref}}} - 1. \quad (26)$$

This factor represents the relative difference between constraints on θ_{DE} given priors $\sigma_p(\theta_{\text{OM}})$ and $\sigma_p(\theta_{\text{CP}})$ and the reference ideal case $\sigma(\theta_{\text{DE}})|_{\text{ref}} = \sigma[\theta_{\text{DE}}|0, 0]$ where *nuisance* parameters are perfectly known.

Applying priors of 1% (or 10^{-2} when the fiducial value is zero) on the observable-mass relation parameters but letting the completeness/purity parameters vary freely, the constraints become $(0.009, 0.042)$. Conversely, if we let the observable-mass relation vary freely and apply a 1% prior on the completeness/purity parameters, the constraints become $(0.009, 0.044)$. Finally, applying a 1% prior to all *nuisance* parameters (related to the observational effects), the constraints become $(0.006, 0.041)$. This corresponds to a degradation of (8%, 21%) relative to the case in which these *nuisance* parameters are perfectly known.

External priors may come from multiple sources, including detailed simulations, lensing masses for a subsample of clusters, or cross-matches to clusters detected at other wavelengths, e.g. X-ray and/or millimeter. In all cases, these priors are likely to provide clues on the correct functional forms for these functions and conservative ranges for both the observable-mass relation and the completeness/purity parameters.

Fig. 5 shows Fisher constraints – relative to the fiducial value – for each *nuisance* parameter θ_n . Given that none of these parameters are constrained to better than 10%, having 1% priors on any of these nuisance parameters would have an important effect in constraining the parameters themselves. However, as we have seen the effect on improving dark energy constraints is very small.

Fig. 6 shows contours of constant degradation $\mathcal{D}_{\theta_{\text{DE}}}$ on dark energy parameters $\theta_{\text{DE}} = (\Omega_{\text{DE}}, w)$ – relative to perfect *nuisance* parameters – as a function of priors on observable-mass relation $\sigma_p(\theta_{\text{OM}})$ and on completeness/purity parameters $\sigma_p(\theta_{\text{CP}})$. Notice that both panels of Fig. 6 present a similar qualitative behavior, though constraints on w do not degrade as much as constraints on Ω_{DE} . We see that it is important to improve priors on both observable-mass as well as completeness/purity parameters. For degradations on dark energy constraints to remain lower than 20%, it is necessary to have quite strong external priors at the subpercent level, which are clearly very hard to achieve even in optimistic scenarios.

C. Future Surveys

Future surveys [58–60], will allow for improvements on both total survey area and depth and the effects of completeness and purity across these improvements tend to become more important. The impact of survey depth or maximum redshift z_{max} on dark energy constraints is shown in Fig. 7 and Table III.

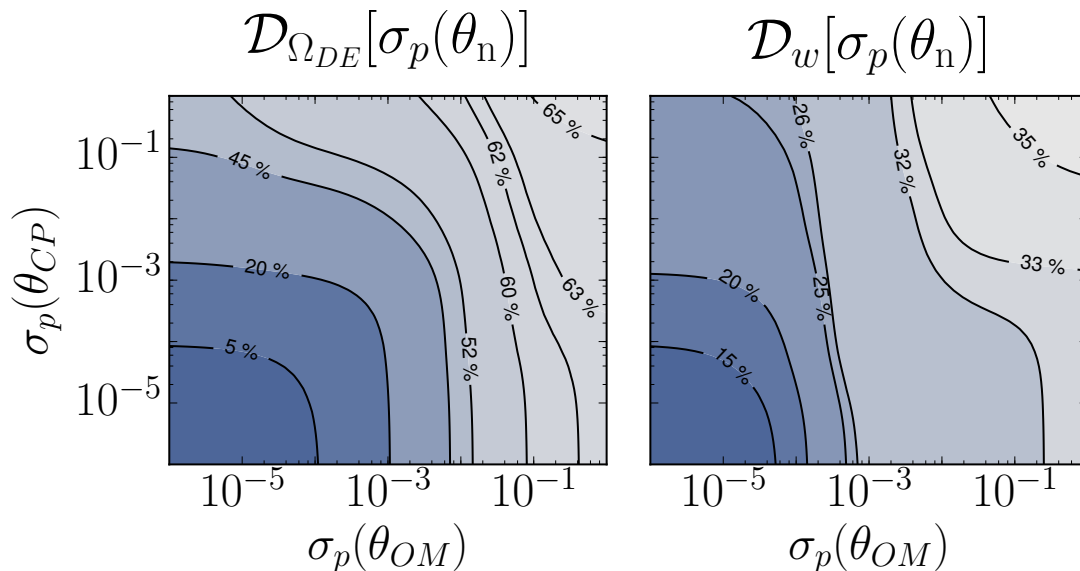


FIG. 6. Contours of constant degradation $\mathcal{D}_{\theta_{DE}}$ on constraints of dark energy parameters $\theta_{DE} = (\Omega_{DE}, w)$ as a function of priors $\sigma_p(\theta_{OM})$ on all observable-mass relation parameters and priors $\sigma_p(\theta_{CP})$ on all completeness/purity parameters. The degradation is considered for case (1) and relative to the case of perfect *nuisance* parameters (for which $\sigma_p(\theta_{OM}) = \sigma_p(\theta_{CP}) = 0$). For $\mathcal{D}_{\theta_{DE}} < 20\%$, subpercent level priors on all *nuisance* parameters are required.

z_{max}	Case (1)		Case (2)	
	$\sigma(\Omega_{DE})$	$\sigma(w)$	$\sigma(\Omega_{DE})$	$\sigma(w)$
0.3	0.033	0.201	0.051	0.254
0.5	0.018	0.089	0.025	0.100
0.7	0.014	0.068	0.017	0.077
1.0	0.010	0.046	0.012	0.049
1.2	0.009	0.040	0.010	0.044
1.5	0.008	0.035	0.010	0.039
1.7	0.008	0.034	0.009	0.037
2.0	0.008	0.033	0.009	0.035

TABLE III. Constraints for dark energy as a function of maximum redshift z_{max} . Here all *nuisance* parameters describing the effective selection function (observable-mass, completeness and purity) vary freely.

Optical cluster finders applied to the SDSS in the last decade were limited to relatively shallow magnitudes. For instance the MaxBCG cluster catalog [24] had $z_{max} = 0.3$, which in our Fisher analysis produces constraints $\sigma(\Omega_{DE}, w) = (0.033, 0.201)$, corresponding to a degradation of (235%, 341%) relative to our fiducial case ($z_{max} = 1.0$). More recently, the redMaPPer cluster finder [26, 27] has been applied to both the SDSS and the DES Science Verification data, producing catalogs that go up to $z_{max} \sim 0.7$, corresponding to constraints of (0.014, 0.068), a degradation of (43%, 48%) relative to our fiducial model. Since redMaPPer makes use of the red sequence for detecting optical clusters, it may be challenging to extend its results to redshifts much larger

than these.

For upcoming surveys planned to extend observations to higher redshifts, we find constraints of (0.008, 0.033) for $z_{max} = 2$, an improvement of (22%, 28%). Case (2) presents a higher degradation when lowering z_{max} than case (1), however, the improvement is lower when we extend z_{max} .

We now quantify the impact of completeness and purity for different values of z_{max} by considering the degradation $\mathcal{D}_{\theta_{DE}}$ on dark energy constraints from Eq. 26, for the case with free completeness and purity parameters $\sigma[\Omega_{DE}|\sigma_p(\theta_{CP}) = \infty]$ relative to the case of perfect knowledge $\sigma[\Omega_{DE}|\sigma_p(\theta_{CP}) = 0]$. In Fig. 8 we see that $\mathcal{D}_{\theta_{DE}}$ has a significant overall improvement (i.e. decrease) with the increase of z_{max} for cases (1,2), up to $z_{max} \sim 1.0 - 1.2$. Beyond those redshifts, the degradation increases again, especially for w in case (1). Notice however that these higher degradations are on top of much improved dark energy constraints (see Table III). Therefore to fully exploit improvements on cluster dark energy constraints coming from larger survey depths, it will be important to properly account for selection effects, despite the fact that it may be significantly harder to quantify these effects at these higher redshifts.

Finally we quantify the effect of changes in survey area. We keep our approach of considering sample covariance from cells of 10 deg^2 and notice that the Fisher Matrix has a linear dependence on total area. This means all constrained parameters have the same degradation/improvements due changes on the survey area. Our fiducial area of 5000 deg^2 is similar to what will be observed by the DES. An area twice as large (1/4 of sky)

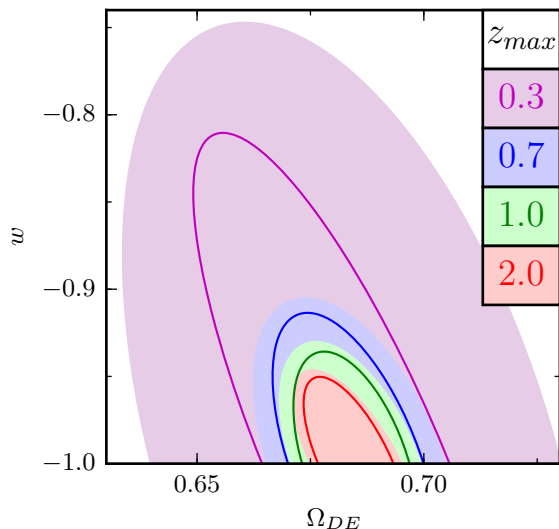


FIG. 7. Effect on dark energy constraints when changing the survey maximum redshift z_{max} from 0.3 (pink), 0.7 (blue), 1.0 (green) and 2.0 (red). Solid lines refer to case (1) and shaded regions refer to case (2).

results in an improvement of $\sim 29\%$ on both dark energy constraints. For half-sky observations, constraints improve by $\sim 50\%$, and for full-sky they improve by $\sim 65\%$.

VII. DISCUSSION

We have explored the effects of completeness and purity on dark energy constraints from the abundance and clustering of galaxy clusters. We parametrized the selection of cluster samples to reflect a decrease in completeness and purity at lower masses such that they both reach $\sim 50\%$ at a mass scale $M \sim 10^{13.5} M_{\odot}/h$. The ratio (c/p) determines the effective selection. Within our parametrization, (c/p) either goes to zero (case 1) or infinity (case 2) as $M \rightarrow 0$.

We first considered the bias induced on dark energy constraints when neglecting completeness and purity effects from cases (1) and (2). We found that the bias becomes comparable to dark energy constraints at a threshold mass of $M_{th}^{obs} \sim 10^{14.2} M_{\odot}/h$. As this represents the minimum threshold for which it is safe to ignore selection effects, we then proceeded to study the inclusion of completeness and purity parameters in dark energy constraints for a lower fiducial mass threshold of $M_{th}^{obs} \sim 10^{13.8} M_{\odot}/h$.

Since the effective selection includes not only completeness and purity but also the observable-mass distribution, the impact of including completeness and purity depends on assumptions made for the observable-mass parameters. Within case (1), baseline constraints for fixed observable-mass parameters and fixed complete-

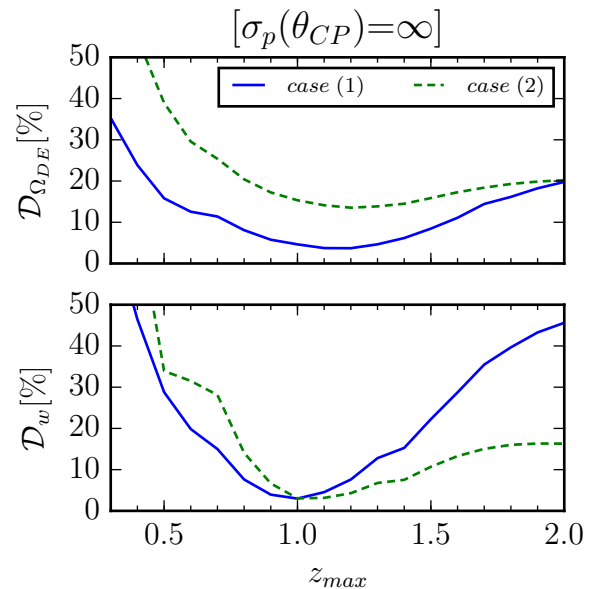


FIG. 8. Percent degradation $\mathcal{D}_{\theta_{DE}}$ on constraints for dark energy parameters $\theta_{DE} = (\Omega_{DE}, w)$ as a function of maximum redshift z_{max} , for selection function parametrized in case (1) (solid line) and case (2) (dashed line). Degradations are computed for the case where the completeness and purity parameters are free $[\sigma_p(\theta_{CP}) = \infty]$ relative to the case where these parameters are perfectly known $[\sigma_p(\theta_{CP}) = 0]$. $\mathcal{D}_{\theta_{DE}}$ decreases with z_{max} up to $z_{max} \sim 1$ and increases for higher redshifts. The dark energy constraints themselves always improve for higher values of z_{max} , but the relative sensitivity to knowledge on selection parameters increases.

ness and purity are $\sigma(\Omega_{DE}, w) = (0.006, 0.033)$ and when only completeness and purity parameters vary freely, these degrade to $(0.009, 0.042)$. On the other hand, if observable-mass parameters vary freely whereas completeness and purity parameters remain fixed, constraints are $\sigma(\Omega_{DE}, w) = (0.009, 0.044)$ and they only degrade to $(0.010, 0.046)$ if completeness and purity also vary freely.

Next we considered the impact of external priors on observable-mass and completeness/purity parameters. From the perspective of dark energy constraints these are *nuisance* parameters (related to the observational effects). We find that joint priors on all *nuisance* parameters need to be known to better than 1% in order to improve dark energy constraints significantly; with these priors, constraints are restored to $\sigma(\Omega_{DE}, w) = (0.006, 0.041)$ for case (1).

Although it seems unlikely that external priors on selection parameters will reach sub-percent levels for current and upcoming clusters surveys, interesting priors should be possible from a combination of multiple sources, including detailed simulations, cross-matches from other surveys and follow-up spectroscopic observations for a fraction of the cluster sample. For instance, the DES has developed detailed simulations that mimic all its observational properties [61, 62]. By running op-

tical cluster finders on these simulations, it is possible to characterize observable-mass and completeness/purity functions [46]. Moreover, DES has a significant overlap with the South Pole Telescope (SPT), so cross-matches of DES optical clusters and SPT SZ clusters allow for calibrations on the observable-mass relation [38]. A similar calibration can be achieved from X-ray detections [63, 64] and lensing masses [65].

Even though our results indicate that only very stringent (and hard to achieve) priors on *nuisance* parameters would be effective in improving dark energy constraints from self-calibrated constraints (where the *nuisance* parameters were constrained along the cosmology), such priors are actually very important for checking the validity of the assumed functional forms, providing consistency checks for internal self-calibration of *nuisance* parameters.

We also investigated the effect of changing survey area (from our fiducial $\Delta\Omega = 5000 \text{ deg}^2$) and maximum redshift (from fiducial $z_{max} = 1.0$), reflecting expectations from future surveys. For $\Delta\Omega = 10000 \text{ deg}^2$ (1/4 of sky) the constraints would improve by $\sim 29\%$ and for $\Delta\Omega = 40,000 \text{ deg}^2$ (full-sky) by $\sim 65\%$, relative to the fiducial case. If we expand the maximum redshift to $z_{max} = 2.0$, constraints on (Ω_{DE}, w) improve by (22%, 28%) on for case (1), though most of this improvement is already achieved for $z_{max} = 1.5$. Despite the improvements on the constraints for higher redshifts and survey areas, these constraints also degrade more significantly in the lack of knowledge of selection parameters. Therefore to fully exploit the gain in precision, it will be even more important to better understand and calibrate the cluster selection function.

Our results were based on the parametrized functions chosen for the effective selection, and they may depend to some extent on these choices. We proposed functional forms for completeness and purity, which are inspired by ongoing work involving runs of cluster finders on DES simulations, which we will present elsewhere [46]. In fact, our parametrizations bracket a considerable range of possibilities, so we do not expect significant changes in our conclusions when considering alternative parametrizations. On the other hand, when extending cluster analyses to significantly lower mass thresholds, one needs to be assured that the functional forms are still valid down to those masses, which may be hard even with simulations and multi-wavelength cross-matches. In particular, as c/p become lower than 50%, we probably need to consider more general functions (or even an arbitrary behavior) for completeness and purity, which may then significantly degrade dark energy constraints (or even bias them for an oversimplified selection), despite the increase in the number of clusters probed. Again, we envision that detailed simulations and cross-matches should help us in defining the most appropriate parametrizations.

Given that the halo mass-function must be known to high precision for cosmological applications [66, 67], and the fact that the Tinker mass-function is only precise at the 5% level [50], we investigated the effect of changing the halo mass-function prescription in our analysis. In real-data analysis one is expected to make use of well-calibrated fitting formulae or emulators for the mass-function (see e.g. [67]). For illustrative purposes we replaced the Tinker mass-function by the fitting formula from Jenkins [68] We found that this change on the mass function causes variations of up to 20% on the number counts, which leads to changes $\leq 30\%$ on the cosmological constraints and $\leq 80\%$ on the constraints of nuisance parameters. However, the degradation effects on the dark energy constraints caused by the inclusion of nuisance parameters remain comparable to when we use the Tinker mass function (the largest degradation occurs when one of the two sets of nuisance parameters θ_{OM} or θ_{CP} is introduced, and the inclusion of the second set is negligible), as does the bias on dark energy parameters introduced by ignoring selection function effects. Therefore, the main conclusions regarding inclusion/exclusion of nuisance parameters are the same as those presented throughout this work.

Although intrinsic degeneracies always remain to some extent, further improvements in the theoretical modeling of cluster properties coming from N-body and gas-dynamics simulations will improve our knowledge of the halo mass-function and bias in the presence of baryonic effects [69, 70], and help define appropriate functional forms for the observable-mass relation and its intrinsic scatter [31–33]. Improvements on semi-analytical Halo Occupation Distribution models will also allow for the creation of reliable mock galaxy catalogs on which we may run cluster finders and calibrate cluster selection parameters. These theoretical developments combined with external calibrations from cluster cross-matches are essential for cluster cosmology. The self-consistency between observations and theory predictions – which account for all relevant observational effects – will advance our knowledge of the astrophysical processes that regulate observed cluster properties and simultaneously lead to trustworthy cluster cosmological constraints.

ACKNOWLEDGMENTS

We thank Christophe Benoist, Vinicius Busti, Ricardo Ogando and Luiz da Costa for useful discussions. MA is supported by FAPESP. ML is partially supported by FAPESP and CNPq.

- [1] M. Boylan-Kolchin, V. Springel, S. D. M. White, A. Jenkins, and G. Lemson, *Mon. Not. R. Astron. Soc.* **398**, 1150 (2009), arXiv:0903.3041 [astro-ph.CO].
- [2] A. A. Klypin, S. Trujillo-Gomez, and J. Primack, *Astrophys. J.* **740**, 102 (2011), arXiv:1002.3660.
- [3] A. Klypin, G. Yepes, S. Gottlöber, F. Prada, and S. Heß, *Mon. Not. R. Astron. Soc.* **457**, 4340 (2016), arXiv:1411.4001.
- [4] P. Fosalba, M. Crocce, E. Gaztañaga, and F. J. Castander, *Mon. Not. R. Astron. Soc.* **448**, 2987 (2015), arXiv:1312.1707.
- [5] M. Crocce, F. J. Castander, E. Gaztañaga, P. Fosalba, and J. Carretero, *Mon. Not. R. Astron. Soc.* **453**, 1513 (2015), arXiv:1312.2013.
- [6] P. Fosalba, E. Gaztañaga, F. J. Castander, and M. Crocce, *Mon. Not. R. Astron. Soc.* **447**, 1319 (2015), arXiv:1312.2947.
- [7] F. Schmidt, M. Lima, H. Oyaizu, and W. Hu, *Phys. Rev. D* **79**, 083518 (2009), arXiv:0812.0545.
- [8] M. Lima and W. Hu, *Phys. Rev. D* **70**, 043504 (2004), astro-ph/0401559.
- [9] M. Lima and W. Hu, *Phys. Rev. D* **72**, 043006 (2005), astro-ph/0503363.
- [10] M. Lima and W. Hu, *Phys. Rev. D* **76**, 123013 (2007), arXiv:0709.2871.
- [11] H.-Y. Wu, E. Rozo, and R. H. Wechsler, *Astrophys. J.* **688**, 729-741 (2008), arXiv:0803.1491.
- [12] B. M. S. Erickson, C. E. Cunha, and A. E. Evrard, *Phys. Rev. D* **84**, 103506 (2011), arXiv:1106.3067 [astro-ph.CO].
- [13] E. Rozo, E. Rykoff, B. Koester, B. Nord, H.-Y. Wu, A. Evrard, and R. Wechsler, *Astrophys. J.* **740**, 53 (2011), arXiv:1104.2090.
- [14] B. Ascaso, N. Benítez, R. Dupke, E. Cypriano, G. Limaneto, C. López-Sanjuan, J. Varela, J. S. Alcaniz, T. Broadhurst, A. J. Cenarro, N. C. Devi, L. A. Díaz-García, C. A. C. Fernandes, C. Hernández-Montegudo, S. Mei, C. Mendes de Oliveira, A. Molino, I. Oteo, W. Schoenell, L. Sodré, K. Viironen, and A. Marín-Franch, *Mon. Not. R. Astron. Soc.* **456**, 4291 (2016), arXiv:1601.00656.
- [15] B. Ascaso, S. Mei, J. G. Bartlett, and N. Benítez, *Mon. Not. R. Astron. Soc.* (2016), 10.1093/mnras/stw2508, arXiv:1605.07620.
- [16] E. S. Levine, A. E. Schulz, and M. White, *Astrophys. J.* **577**, 569 (2002), astro-ph/0204273.
- [17] S. Majumdar and J. J. Mohr, *Astrophys. J.* **613**, 41 (2004), astro-ph/0305341.
- [18] M. D. Gladders, H. K. C. Yee, S. Majumdar, L. F. Barrientos, H. Hoekstra, P. B. Hall, and L. Infante, *Astrophys. J.* **655**, 128 (2007), astro-ph/0603588.
- [19] C. E. Cunha, *Cross-calibration of cluster mass-observables and dark energy*, Ph.D. thesis, The University of Chicago (2008).
- [20] C. Cunha, *Phys. Rev. D* **79**, 063009 (2009), arXiv:0812.0583.
- [21] E. Rozo, R. H. Wechsler, E. S. Rykoff, J. T. Annis, M. R. Becker, A. E. Evrard, J. A. Frieman, S. M. Hansen, J. Hao, D. E. Johnston, B. P. Koester, T. A. McKay, E. S. Sheldon, and D. H. Weinberg, *Astrophys. J.* **708**, 645 (2010), arXiv:0902.3702 [astro-ph.CO].
- [22] B. A. Benson, T. de Haan, J. P. Dudley, C. L. Reichardt, K. A. Aird, K. Andersson, R. Armstrong, M. L. N. Ashby, M. Bautz, M. Bayliss, G. Bazin, L. E. Bleem, M. Brodwin, J. E. Carlstrom, C. L. Chang, H. M. Cho, A. Clocchiatti, T. M. Crawford, A. T. Crites, S. Desai, M. A. Dobbs, R. J. Foley, W. R. Forman, E. M. George, M. D. Gladders, A. H. Gonzalez, N. W. Halverson, N. Harrington, F. W. High, G. P. Holder, W. L. Holzapfel, S. Hoover, J. D. Hrubes, C. Jones, M. Joy, R. Keisler, L. Knox, A. T. Lee, E. M. Leitch, J. Liu, M. Lueker, D. Luong-Van, A. Mantz, D. P. Marrone, M. McDonald, J. J. McMahon, J. Mehl, S. S. Meyer, L. Mocuano, J. J. Mohr, T. E. Montroy, S. S. Murray, T. Natoli, S. Padin, T. Plagge, C. Pryke, A. Rest, J. Ruel, J. E. Ruhl, B. R. Saliwanchik, A. Saro, J. T. Sayre, K. K. Schaffer, L. Shaw, E. Shirokoff, J. Song, H. G. Spieler, B. Stalder, Z. Staniszewski, A. A. Stark, K. Story, C. W. Stubbs, R. Suhada, A. van Engelen, K. Vanderlinde, J. D. Vieira, A. Vikhlinin, R. Williamson, O. Zahn, and A. Zenteno, *Astrophys. J.* **763**, 147 (2013), arXiv:1112.5435 [astro-ph.CO].
- [23] Planck Collaboration, P. A. R. Ade, N. Aghanim, C. Armitage-Caplan, M. Arnaud, M. Ashdown, F. Atrio-Barandela, J. Aumont, C. Baccigalupi, A. J. Banday, and et al., *Astron. Astrophys.* **571**, A20 (2014), arXiv:1303.5080.
- [24] B. P. Koester, T. A. McKay, J. Annis, R. H. Wechsler, A. E. Evrard, E. Rozo, L. Bleem, E. S. Sheldon, and D. Johnston, *Astrophys. J.* **660**, 221 (2007), astro-ph/0701268.
- [25] S. Farrens, F. B. Abdalla, E. S. Cypriano, C. Sabiu, and C. Blake, *Mon. Not. R. Astron. Soc.* **417**, 1402 (2011), arXiv:1106.5687.
- [26] E. S. Rykoff, E. Rozo, M. T. Busha, C. E. Cunha, A. Finoguenov, A. Evrard, J. Hao, B. P. Koester, A. Leauthaud, B. Nord, M. Pierre, R. Reddick, T. Sadibekova, E. S. Sheldon, and R. H. Wechsler, *Astrophys. J.* **785**, 104 (2014), arXiv:1303.3562.
- [27] E. S. Rykoff, E. Rozo, D. Hollowood, A. Bermeo-Hernandez, T. Jeltema, J. Mayers, A. K. Romer, P. Rooney, A. Saro, C. Vergara Cervantes, R. H. Wechsler, H. Wilcox, T. M. C. Abbott, F. B. Abdalla, S. Allam, J. Annis, A. Benoit-Lévy, G. M. Bernstein, E. Bertin, D. Brooks, D. L. Burke, D. Capozzi, A. Carnero Rosell, M. Carrasco Kind, F. J. Castander, M. Childress, C. A. Collins, C. E. Cunha, C. B. D'Andrea, L. N. da Costa, T. M. Davis, S. Desai, H. T. Diehl, J. P. Dietrich, P. Doel, A. E. Evrard, D. A. Finley, B. Flaugher, P. Fosalba, J. Frieman, K. Glazebrook, D. A. Goldstein, D. Gruen, R. A. Gruendl, G. Gutierrez, M. Hilton, K. Honscheid, B. Hoyle, D. J. James, S. T. Kay, K. Kuehn, N. Kuropatkin, O. Lahav, G. F. Lewis, C. Lidman, M. Lima, M. A. G. Maia, R. G. Mann, J. L. Marshall, P. Martini, P. Melchior, C. J. Miller, R. Miquel, J. J. Mohr, R. C. Nichol, B. Nord, R. Ogando, A. A. Plazas, K. Reil, M. Sahlén, E. Sanchez, B. Santiago, V. Scarpine, M. Schubnell, I. Sevilla-Noarbe, R. C. Smith, M. Soares-Santos, F. Sobreira, J. P. Stott, E. Suchyta, M. E. C. Swanson, G. Tarle, D. Thomas, D. Tucker, S. Uddin, P. T. P. Viana, V. Vikram, A. R. Walker, Y. Zhang, and DES Collaboration, *Astro-*

- phys. J. Supp. **224**, 1 (2016), arXiv:1601.00621.
- [28] J. P. Dietrich, Y. Zhang, J. Song, C. P. Davis, T. A. McKay, L. Baruah, M. Becker, C. Benoist, M. Busha, L. A. N. da Costa, J. Hao, M. A. G. Maia, C. J. Miller, R. Ogando, A. K. Romer, E. Rozo, E. Rykoff, and R. Wechsler, *Mon. Not. R. Astron. Soc.* **443**, 1713 (2014), arXiv:1405.2923.
- [29] M. Soares-Santos, R. R. de Carvalho, J. Annis, R. R. Gal, F. La Barbera, P. A. A. Lopes, R. H. Wechsler, M. T. Busha, and B. F. Gerke, *Astrophys. J.* **727**, 45 (2011), arXiv:1011.3458 [astro-ph.CO].
- [30] C. J. Miller, R. C. Nichol, D. Reichart, R. H. Wechsler, A. E. Evrard, J. Annis, T. A. McKay, N. A. Bahcall, M. Bernardi, H. Boehringer, A. J. Connolly, T. Goto, A. Kniazev, D. Lamb, M. Postman, D. P. Schneider, R. K. Sheth, and W. Voges, *Astron. J.* **130**, 968 (2005), astro-ph/0503713.
- [31] D. Nagai, *Astrophys. J.* **650**, 538 (2006), astro-ph/0512208.
- [32] A. V. Kravtsov, A. Vikhlinin, and D. Nagai, *Astrophys. J.* **650**, 128 (2006), astro-ph/0603205.
- [33] D. Nagai, A. Vikhlinin, and A. V. Kravtsov, *Astrophys. J.* **655**, 98 (2007), astro-ph/0609247.
- [34] L. Old, R. Wojtak, G. A. Mamon, R. A. Skibba, F. R. Pearce, D. Croton, S. Bamford, P. Behroozi, R. de Carvalho, J. C. Muñoz-Cuartas, D. Gifford, M. E. Gray, A. von der Linden, M. R. Merrifield, S. I. Muldrew, V. Müller, R. J. Pearson, T. J. Ponman, E. Rozo, E. Rykoff, A. Saro, T. Sepp, C. Sifón, and E. Tempel, *Mon. Not. R. Astron. Soc.* **449**, 1897 (2015), arXiv:1502.07347.
- [35] L. Yu, K. Nelson, and D. Nagai, *Astrophys. J.* **807**, 12 (2015), arXiv:1501.00317.
- [36] M. Bonamente, M. Joy, S. J. LaRoque, J. E. Carlstrom, D. Nagai, and D. P. Marrone, *Astrophys. J.* **675**, 106-114 (2008), arXiv:0708.0815.
- [37] E. S. Rykoff, T. A. McKay, M. R. Becker, A. Evrard, D. E. Johnston, B. P. Koester, E. Rozo, E. S. Sheldon, and R. H. Wechsler, *Astrophys. J.* **675**, 1106-1124 (2008), arXiv:0709.1158.
- [38] A. Saro, S. Bocquet, E. Rozo, B. A. Benson, J. Mohr, E. S. Rykoff, M. Soares-Santos, L. Bleem, S. Dodelson, P. Melchior, F. Sobreira, V. Upadhyay, J. Weller, T. Abbott, F. B. Abdalla, S. Allam, R. Armstrong, M. Banerji, A. H. Bauer, M. Bayliss, A. Benoit-Lévy, G. M. Bernstein, E. Bertin, M. Brodwin, D. Brooks, E. Buckley-Geer, D. L. Burke, J. E. Carlstrom, R. Capasso, D. Capozzi, A. Carnero Rosell, M. Carrasco Kind, I. Chiu, R. Covarrubias, T. M. Crawford, M. Crocce, C. B. D'Andrea, L. N. da Costa, D. L. DePoy, S. Desai, T. de Haan, H. T. Diehl, J. P. Dietrich, P. Doel, C. E. Cunha, T. F. Eifler, A. E. Evrard, A. Fausti Neto, E. Fernandez, B. Flaugher, P. Fosalba, J. Frieman, C. Gangkofner, E. Gaztanaga, D. Gerdes, D. Gruen, R. A. Gruendl, N. Gupta, C. Hennig, W. L. Holzappel, K. Honscheid, B. Jain, D. James, K. Kuehn, N. Kuropatkin, O. Lahav, T. S. Li, H. Lin, M. A. G. Maia, M. March, J. L. Marshall, P. Martini, M. McDonald, C. J. Miller, R. Miquel, B. Nord, R. Ogando, A. A. Plazas, C. L. Reichardt, A. K. Romer, A. Roodman, M. Sako, E. Sanchez, M. Schubnell, I. Sevilla, R. C. Smith, B. Stalder, A. A. Stark, V. Strazzullo, E. Suchyta, M. E. C. Swanson, G. Tarle, J. Thaler, D. Thomas, D. Tucker, V. Vikram, A. von der Linden, A. R. Walker, R. H. Wechsler, W. Wester, A. Zenteno, and K. E. Ziegler, *Mon. Not. R. Astron. Soc.* **454**, 2305 (2015), arXiv:1506.07814.
- [39] M. R. Becker and A. V. Kravtsov, *Astrophys. J.* **740**, 25 (2011), arXiv:1011.1681 [astro-ph.CO].
- [40] D. Gruen, S. Seitz, F. Brimiouille, R. Kosyra, J. Koppenhoefer, C.-H. Lee, R. Bender, A. Riffeser, T. Eichner, T. Weidinger, and M. Bierschenk, *Mon. Not. R. Astron. Soc.* **442**, 1507 (2014), arXiv:1310.6744.
- [41] A. von der Linden, A. Mantz, S. W. Allen, D. E. Applegate, P. L. Kelly, R. G. Morris, A. Wright, M. T. Allen, P. R. Burchat, D. L. Burke, D. Donovan, and H. Ebeling, *Mon. Not. R. Astron. Soc.* **443**, 1973 (2014), arXiv:1402.2670.
- [42] A. von der Linden, M. T. Allen, D. E. Applegate, P. L. Kelly, S. W. Allen, H. Ebeling, P. R. Burchat, D. L. Burke, D. Donovan, R. G. Morris, R. Blandford, T. Erben, and A. Mantz, *Mon. Not. R. Astron. Soc.* **439**, 2 (2014), arXiv:1208.0597.
- [43] J. P. Dietrich, Y. Zhang, J. Song, C. P. Davis, T. A. McKay, L. Baruah, M. Becker, C. Benoist, M. Busha, L. A. N. da Costa, J. Hao, M. A. G. Maia, C. J. Miller, R. Ogando, A. K. Romer, E. Rozo, E. Rykoff, and R. Wechsler, *Mon. Not. R. Astron. Soc.* **443**, 1713 (2014), arXiv:1405.2923.
- [44] N. Battaglia, A. Leauthaud, H. Miyatake, M. Hasselfield, M. B. Gralla, R. Allison, J. R. Bond, E. Calabrese, D. Crichton, M. J. Devlin, J. Dunkley, R. Dünner, T. Erben, S. Ferrara, M. Halpern, M. Hilton, J. C. Hill, A. D. Hincks, R. Hložek, K. M. Huffenberger, J. P. Hughes, J. P. Kneib, A. Kosowsky, M. Makler, T. A. Marriage, F. Menanteau, L. Miller, K. Moodley, B. Moraes, M. D. Niemack, L. Page, H. Shan, N. Sehgal, B. D. Sherwin, J. L. Sievers, C. Sifón, D. N. Spergel, S. T. Staggs, J. E. Taylor, R. Thornton, L. van Waerbeke, and E. J. Wollack, *Journal of Cosmology and Astroparticle Physics* **8**, 013 (2016), arXiv:1509.08930.
- [45] M. Penna-Lima, J. G. Bartlett, E. Rozo, J.-B. Melin, J. Merten, A. E. Evrard, M. Postman, and E. Rykoff, *ArXiv e-prints* (2016), arXiv:1608.05356.
- [46] M. Aguena *et al.*, (in prep.).
- [47] H. Oyaizu, M. Lima, C. E. Cunha, H. Lin, J. Frieman, and E. S. Sheldon, *Astrophys. J.* **674**, 768-783 (2008), arXiv:0708.0030.
- [48] F. B. Abdalla, M. Banerji, O. Lahav, and V. Rashkov, *Mon. Not. R. Astron. Soc.* **417**, 1891 (2011), arXiv:0812.3831.
- [49] C. Sánchez, M. Carrasco Kind, H. Lin, R. Miquel, F. B. Abdalla, A. Amara, M. Banerji, C. Bonnett, R. Brunner, D. Capozzi, A. Carnero, F. J. Castander, L. A. N. da Costa, C. Cunha, A. Fausti, D. Gerdes, N. Greisel, J. Gschwend, W. Hartley, S. Jouvel, O. Lahav, M. Lima, M. A. G. Maia, P. Martí, R. L. C. Ogando, F. Ostrowski, P. Pellegrini, M. M. Rau, I. Sadeh, S. Seitz, I. Sevilla-Noarbe, A. Sypniewski, J. de Vicente, T. Abbot, S. S. Allam, D. Atlee, G. Bernstein, J. P. Bernstein, E. Buckley-Geer, D. Burke, M. J. Childress, T. Davis, D. L. DePoy, A. Dey, S. Desai, H. T. Diehl, P. Doel, J. Estrada, A. Evrard, E. Fernández, D. Finley, B. Flaugher, J. Frieman, E. Gaztanaga, K. Glazebrook, K. Honscheid, A. Kim, K. Kuehn, N. Kuropatkin, C. Lidman, M. Makler, J. L. Marshall, R. C. Nichol, A. Roodman, E. Sánchez, B. X. Santiago, M. Sako, R. Scalzo, R. C. Smith, M. E. C. Swanson, G. Tarle, D. Thomas, D. L. Tucker, S. A. Uddin, F. Valdés, A. Walker, F. Yuan,

- and J. Zuntz, *Mon. Not. R. Astron. Soc.* **445**, 1482 (2014), arXiv:1406.4407 [astro-ph.IM].
- [50] J. Tinker, A. V. Kravtsov, A. Klypin, K. Abazajian, M. Warren, G. Yepes, S. Gottlöber, and D. E. Holz, *Astrophys. J.* **688**, 709-728 (2008), arXiv:0803.2706.
- [51] E. J. Baxter, E. Rozo, B. Jain, E. Rykoff, and R. H. Wechsler, *Mon. Not. R. Astron. Soc.* **463**, 205 (2016), arXiv:1604.00048.
- [52] J. L. Tinker, B. E. Robertson, A. V. Kravtsov, A. Klypin, M. S. Warren, G. Yepes, and S. Gottlöber, *Astrophys. J.* **724**, 878 (2010), arXiv:1001.3162.
- [53] W. Hu and A. V. Kravtsov, *Astrophys. J.* **584**, 702 (2003), astro-ph/0203169.
- [54] W. Hu and A. V. Kravtsov, *Astrophys. J.* **584**, 702 (2003), astro-ph/0203169.
- [55] A. Amara and A. Réfrégier, *Mon. Not. R. Astron. Soc.* **391**, 228 (2008), arXiv:0710.5171.
- [56] Planck Collaboration, P. A. R. Ade, N. Aghanim, M. Arnaud, M. Ashdown, J. Aumont, C. Baccigalupi, A. J. Banday, R. B. Barreiro, J. G. Bartlett, and et al., *ArXiv e-prints* (2015), arXiv:1502.01589.
- [57] The Dark Energy Survey Collaboration, *ArXiv Astrophysics e-prints* (2005), astro-ph/0510346.
- [58] “eROSITA,” <http://www.mpe.mpg.de/eROSITA>.
- [59] “Euclid,” <http://www.euclid-ec.org>.
- [60] “LSST,” <http://www.lsst.org>.
- [61] Y. Park, E. Krause, S. Dodelson, B. Jain, A. Amara, M. R. Becker, S. L. Bridle, J. Clampitt, M. Crocce, P. Fosalba, E. Gaztanaga, K. Honscheid, E. Rozo, F. Sobreira, C. Sánchez, R. H. Wechsler, T. Abbott, F. B. Abdalla, S. Allam, A. Benoit-Lévy, E. Bertin, D. Brooks, E. Buckley-Geer, D. L. Burke, A. Carnero Rosell, M. Carrasco Kind, J. Carretero, F. J. Castander, L. N. da Costa, D. L. DePoy, S. Desai, J. P. Dietrich, P. Doel, T. F. Eifler, A. Fausti Neto, E. Fernandez, D. A. Finley, B. Flaugher, D. W. Gerdes, D. Gruen, R. A. Gruendl, G. Gutierrez, D. J. James, S. Kent, K. Kuehn, N. Kuropatkin, M. Lima, M. A. G. Maia, J. L. Marshall, P. Melchior, C. J. Miller, R. Miquel, R. C. Nichol, R. Ogando, A. A. Plazas, N. Roe, A. K. Romer, E. S. Rykoff, E. Sanchez, V. Scarpine, M. Schubnell, I. Sevilla-Noarbe, M. Soares-Santos, E. Suchyta, M. E. C. Swanson, G. Tarle, J. Thaler, V. Vikram, A. R. Walker, J. Weller, J. Zuntz, and DES Collaboration, *Phys. Rev. D* **94**, 063533 (2016), arXiv:1507.05353.
- [62] E. Suchyta, E. M. Huff, J. Aleksić, P. Melchior, S. Jovel, N. MacCrann, A. J. Ross, M. Crocce, E. Gaztanaga, K. Honscheid, B. Leistedt, H. V. Peiris, E. S. Rykoff, E. Sheldon, T. Abbott, F. B. Abdalla, S. Allam, M. Banerji, A. Benoit-Lévy, E. Bertin, D. Brooks, D. L. Burke, A. C. Rosell, M. C. Kind, J. Carretero, C. E. Cunha, C. B. D’Andrea, L. N. da Costa, D. L. DePoy, S. Desai, H. T. Diehl, J. P. Dietrich, P. Doel, T. F. Eifler, J. Estrada, A. E. Evrard, B. Flaugher, P. Fosalba, J. Frieman, D. W. Gerdes, D. Gruen, R. A. Gruendl, D. J. James, M. Jarvis, K. Kuehn, N. Kuropatkin, O. Lahav, M. Lima, M. A. G. Maia, M. March, J. L. Marshall, C. J. Miller, R. Miquel, E. Neilsen, R. C. Nichol, B. Nord, R. Ogando, W. J. Percival, K. Reil, A. Roodman, M. Sako, E. Sanchez, V. Scarpine, I. Sevilla-Noarbe, R. C. Smith, M. Soares-Santos, F. Sobreira, M. E. C. Swanson, G. Tarle, J. Thaler, D. Thomas, V. Vikram, A. R. Walker, R. H. Wechsler, Y. Zhang, and DES Collaboration, *Mon. Not. R. Astron. Soc.* **457**, 786 (2016), arXiv:1507.08336.
- [63] N. Mehtens, A. K. Romer, M. Hilton, E. J. Lloyd-Davies, C. J. Miller, S. A. Stanford, M. Hosmer, B. Hoyle, C. A. Collins, A. R. Liddle, P. T. P. Viana, R. C. Nichol, J. P. Stott, E. N. Dubois, S. T. Kay, M. Sahlén, O. Young, C. J. Short, L. Christodoulou, W. A. Watson, M. Davidson, C. D. Harrison, L. Baruah, M. Smith, C. Burke, J. A. Mayers, P.-J. Deadman, P. J. Rooney, E. M. Edmondson, M. West, H. C. Campbell, A. C. Edge, R. G. Mann, K. Sabirli, D. Wake, C. Benoist, L. da Costa, M. A. G. Maia, and R. Ogando, *Mon. Not. R. Astron. Soc.* **423**, 1024 (2012), arXiv:1106.3056.
- [64] T. Boller, M. J. Freyberg, J. Trümper, F. Haberl, W. Voges, and K. Nandra, *Astron. Astrophys.* **588**, A103 (2016), arXiv:1609.09244 [astro-ph.HE].
- [65] P. Melchior, D. Gruen, T. McClintock, T. N. Varga, E. Sheldon, E. Rozo, A. Amara, M. R. Becker, B. A. Benson, A. Bermeo, S. L. Bridle, J. Clampitt, J. P. Dietrich, W. G. Hartley, D. Hollowood, B. Jain, M. Jarvis, T. Jeltema, T. Kacprzak, N. MacCrann, E. S. Rykoff, A. Saro, E. Suchyta, M. A. Troxel, J. Zuntz, C. Bonnett, A. A. Plazas, T. M. C. Abbott, F. B. Abdalla, J. Annis, A. Benoit-Lévy, G. M. Bernstein, E. Bertin, D. Brooks, E. Buckley-Geer, A. Carnero Rosell, M. Carrasco Kind, J. Carretero, C. E. Cunha, C. B. D’Andrea, L. N. da Costa, S. Desai, T. F. Eifler, B. Flaugher, P. Fosalba, J. García-Bellido, E. Gaztanaga, D. W. Gerdes, R. A. Gruendl, J. Gschwend, G. Gutierrez, K. Honscheid, D. J. James, D. Kirk, E. Krause, K. Kuehn, N. Kuropatkin, O. Lahav, M. Lima, M. A. G. Maia, M. March, P. Martini, F. Menanteau, C. J. Miller, R. Miquel, J. J. Mohr, R. C. Nichol, R. Ogando, A. K. Romer, E. Sanchez, V. Scarpine, I. Sevilla-Noarbe, R. C. Smith, M. Soares-Santos, F. Sobreira, M. E. C. Swanson, G. Tarle, D. Thomas, A. R. Walker, J. Weller, and Y. Zhang, *ArXiv e-prints* (2016), arXiv:1610.06890.
- [66] C. E. Cunha and A. E. Evrard, *Phys. Rev. D* **81**, 083509 (2010), arXiv:0908.0526 [astro-ph.CO].
- [67] T. McClintock, E. Rozo, M. R. Becker, J. DeRose, Y.-Y. Mao, S. McLaughlin, J. L. Tinker, R. H. Wechsler, and Z. Zhai, *ArXiv e-prints* (2018), arXiv:1804.05866.
- [68] A. Jenkins, C. S. Frenk, S. D. M. White, J. M. Colberg, S. Cole, A. E. Evrard, H. M. P. Couchman, and N. Yoshida, *Mon. Not. R. Astron. Soc.* **321**, 372 (2001), astro-ph/0005260.
- [69] W. Cui, S. Borgani, K. Dolag, G. Murante, and L. Tornatore, *Mon. Not. R. Astron. Soc.* **423**, 2279 (2012), arXiv:1111.3066.
- [70] S. Bocquet, A. Saro, K. Dolag, and J. J. Mohr, *Mon. Not. R. Astron. Soc.* **456**, 2361 (2016), arXiv:1502.07357.